CrossMark

ORIGINAL PAPER

Structure, thermal behavior, and dielectric properties of new cesium hydrogen sulfate arsenate: $Cs_2(HSO_4)(H_2AsO_4)$

N. Nouiri[1] · K. Jaouadi[1] · T. Mhiri[1] · N. Zouari[1]

Abstract Synthesis and structural characterization by single-crystal X-ray diffraction method, thermal behavior, and electrical proprieties are given for a new compound with a superprotonic phase transition $Cs_2(HSO_4)(H_2AsO_4)$. The title compound crystallizes in the monoclinic system with the $P2_1/n$ space group. The structure contains zigzag chains of hydrogen-bonded anion tetrahedra that extend in the [010] direction. Each tetrahedron is additionally linked to a tetrahedron neighboring chain to give a planar structure with hydrogen-bonded sheets lying parallel to (10$\bar{1}$). The existence of O–H and (S/As)–O bonds in the structure at room temperature has been confirmed by IR and Raman spectroscopy in the frequency ranges 4000–400 cm^{-1} and 1200–50 cm^{-1}, respectively. Differential scanning calorimetry analysis of the superprotonic transition in $Cs_2(HSO_4)(H_2AsO_4)$ showed that the transformation to high temperature phase occurs at 417 K by one-step process. Thermal decomposition of the product takes place at much higher temperatures, with an onset of approximately 534 K. The superprotonic transition was also studied by impedance and modulus spectroscopy techniques. The conductivity in the high temperature phase at 423 K is $1.58 \times 10^{-4}\ \Omega^{-1}\ cm^{-1}$, and the activation energy for the proton transport is 0.28 eV. The conductivity relaxation parameters associated with the high disorder protonic conduction have been examined from analysis of the M"/M"$_{max}$ spectrum measured in a wide temperature range. Transport properties of this material appear to be due to the proton hopping mechanism.

Introduction

The compounds of general formula $MHXO_4$ and $MH_2X'O_4$ (where M is a monovalent cation: K^+, Rb^+, Cs^+; X is S or Se and X' is P or As) seem to be interesting since their high temperature phase exhibits unusually high conductivity [1–3]. Thus, they belong to the family of superionic conductors which are of great interest because of their potential use in various electrochemical devices such as batteries and fuel cells [4–7].

In the last few years, new mixed hydrogen sulfate phosphate [8–11] and hydrogen sulfate arsenate [12] have been synthesized and structurally characterized. Some of these compounds are known to undergo phase transitions to superprotonic or ferroelectric phases [1, 2]. An examination of the literature has shown so far no structural study of the title compound. Many solid acids in this compounds family have been examined as superprotonic conductors. Proton transport in the superionic phase is facilitated by the rapid reorientation of SO_4 groups [13, 14]. Owing to the limited number of structural types known as exhibiting superprotonic behavior, it has been difficult to assess the role of the hydrogen bond network and/or local hydrogen bond geometry in the proton transport and transformation mechanisms.

Following the investigation concerning the synthesis and the crystal structure of $Rb_2(HSO_4)(H_2PO_4)$ and $Cs_2(HSeO_4)(H_2AsO_4)$ compounds [10, 15], we describe in this paper the synthesis and crystal structure of a new cesium hydrogen sulfate arsenate, $Cs_2(HSO_4)(H_2AsO_4)$ denoted (CsHSAs) which is the second compound belonging to the

✉ K. Jaouadi
khaledjaouadi@yahoo.fr

[1] Laboratoire de Physico-chimie de l'Etat Solide, Département de Chimie, Faculté des Sciences de Sfax, Université de Sfax, BP 1171 Route Soukra, km 3,5, 3000 Sfax, Tunisia

Springer

family of compound with general formula $M_2(HSO_4)(H_2AsO_4)$ (M = Cs, Rb, K, Na, NH_4) after the compound $(NH_4)_2(HSO4)(H_2AsO_4)$ [12]. We demonstrate here through some results of calorimetric analysis and through measurements of conductivity using the complex impedance method, all carried at high temperature, that the transition in CsHSAs at 417 K is protonic and accompanied by breaking of the hydrogen bonds.

Experimental details

Crystal growth

Single crystals of $Cs_2(HSO_4)(H_2AsO_4)$ grew from aqueous solutions of cesium carbonate, sulfate acid, and arsenic acid, in which the mole ratio of Cs:SO_4:AsO_4 was fixed in 10:5:5 according to the following reaction:

$$Cs_2CO_3 + H_2SO_4 + H_3AsO_4 \longrightarrow Cs_2(HSO_4)(H_2AsO_4) + H_2O + CO_2 \nearrow$$

Just enough deionized water was added to a mixture of the carbonate and acids to cause dissolution. This resulting solution was kept under ambient conditions which allowed it to evaporate slowly. A few days later, colorless, transparent, and plate-like crystals of $Cs_2(HSO_4)(H_2AsO_4)$ were obtained. It is noted that the compound is stable in air, and its formula is determined by chemical analysis (Table 1) and confirmed by refinement of the crystal structure.

Investigation techniques

X-ray diffraction

Single-crystal X-ray diffraction intensity data were obtained on an Enraf-Nonius Kappa CCD diffractometer using MoKα radiation (λ = 0.71073 Å). Data were collected at room temperature from an as-synthesized specimen measuring $0.23 \times 0.14 \times 0.09$ mm^3 in size. The unit cell parameters optimized by least-squares refinement were calculated and refined using indexation of the collected intensities and revealed CsHSAs to be monoclinic with lattice parameters a = 7.435 (2) Å, b = 7.543 (1) Å, c = 7.598 (3) Å, and β = 100.7 (4)°. The raw intensity data were corrected for Lorenz and polarizing effects before proceeding to the refinement of the structure. An absorption correction was performed by the program SORTAV [16]. Atomic scattering factors were

taken from the International Tables for X-ray crystallography [17]. A total of 4454 reflections were collected in the whole Ewald sphere for $3.8° \leq \theta \leq 30°$ of which 1318 reflections had an intensity of $I > 2\sigma(I)$. An analysis of the systematic absences showed the space group to be $P2_1/n$.

We solved the structure by first location cesium atom position using the SHELXS-97 program [18], and subsequently, the remaining non-hydrogen atoms were deduced from difference Fourier maps during the refinement of the structure with the SHELXL-97 program [19]. The H atoms were located through difference maps with the aid of a calculation of bond distances and angles and on the basis of the results for the refinement of the structure of $Rb_2(HSO_4)(H_2PO_4)$ by neutron powder diffraction [10]. Details of the data collection and structural analysis are presented in Table 2. The atomic coordinates and parameters are given in Tables 3 and 4.

Infrared and Raman spectroscopy

Infrared spectrum was recorded in the range of 4000–400 cm^{-1} with a "Perkin–Elmer FTIR" spectrophotometer 1000 using a sample dispersed in spectroscopically pure KBr pellet. Furthermore, Raman spectra were measured with a LABRAMHR 800 triple monochromator under a ×50 LF objective microscope. A He-Ne ion laser operating at about 20 mW was used (on the sample) as an excitation source (514.5 nm), with a spectral step of 3 cm^{-1}.

Thermal analysis

Thermo-gravimetric (TG) investigations were performed using a multi-module 92 SETARAM analyzer operating from room temperature up to 1098 K at a constant rate of 5 K min^{-1} under flowing argon. Dry argon was used with a flow of 60 ml/min. A powdered sample, 49.28 mg, was spread evenly in a large platinum crucible to avoid mass effects.

Table 1   Results of chemical analysis for $Cs_2(HSO_4)(H_2AsO_4)$

	As (%)	Cs (%)	S (%)
Calculated	14.86	52.76	6.37
Experimental	14.94 (1)[a]	52.69 (2)[b]	6.31 (4)[c]

[a] Determined by volumetric

[b] Determined by atomic absorption

[c] Determined by the ICP/OES method

Table 2 Summary of crystal data, intensity measurements, and refinement parameters for $Cs_2(HSO_4)(H_2AsO_4)$

I. Crystal data	
Formula	$Cs_2(HSO_4)(H_2AsO_4)$
Formula weight	503.82 g.mol^{-1}
Crystal system: monoclinic	Space group: $P2_1/n$
$a = 7.435\ (2)$ Å	$\beta = 100.7\ (4)°$
$b = 7.543\ (1)$ Å	$V = 418.76\ (2)$ Å^3
$c = 7.598\ (3)$ Å	$Z = 2$
$d_{cal} = 3.996: d_{exp} = 4.003$ g.cm^{-3}	$F(000) = 452$
Linear absorption factor:	$\mu = 12.88$ mm^{-1}
Habit	Colorless
Crystal size	$0.23 \times 0.14 \times 0.09$ mm^3
II. Intensity measurements	
Temperature, 293 K	$\lambda(Mo - K_\alpha) = 0.71073$ Å
Diffractometer	Enarf-Nonius Kappa CCD
Monochromator	Graphite plate
Theta range	3.8°–30°
Measurement area:	$-10 \leq h \leq 10; -10 \leq k \leq 10; -11 \leq l \leq 11$
Total reflections = 4454	Independents reflections = 1925
Parameters of thermal agitation	$R_{int} = 0.0086$ et $R_\sigma = 0.0273$
III. Structure determination	
Lorentz and polarization correction	Absorption correction was applied
Structure solution	Direct methods
Refinement method	Full-matrix least squares on F^2
Thermal displacement parameters	Isotropic for H atoms, anisotopic for non-H
Unique reflection included:	1318 with $I > 2\sigma\ (I)$
Refined parameters	67
$(\Delta\rho)min, (\Delta\rho)max$	-1.03 and $-0.91(e/Å^{-3})$
Unweight agreement factor $R_1 = 0.0415$	Weight agreement factor $wR_2 = 0.0837$

$R_1 = (\Sigma[|F_o| - |F_c|]/\Sigma|F_o|$ and $wR_2 = (\Sigma[W(F^2_o - F^2_c)^2]/[W(F^2_o)^2])^{1/2}$

Differential scanning calorimetry (DSC) has been performed on a DSC Mettler TA 4000 between 300 and 1100 K.

Table 3 Fractional atomic coordinates and temperature factors (U$_{iso}$ for H atoms) for $Cs_2(HSO_4)(H_2AsO_4)$ (Esd given in parentheses)

Atoms	X	Y	Z	Ueq	Occupation
Cs	0.8907 (2)	0.8211 (2)	0.7793 (2)	0.0264 (6)	1
As	0.3988 (5)	0.8158 (5)	0.7458 (4)	0.0148 (3)	0.496(3)
S	0.3988 (5)	0.8158 (5)	0.7458 (4)	0.0148 (3)	0504(3)
O1	0.5042 (5)	0.6866 (6)	0.6652 (4)	0.0023 (2)	1
O2	0.5243 (5)	0.9622 (6)	0.8418 (4)	0.0047 (2)	1
O3	0.2961 (8)	0.7343 (7)	0.8804 (7)	0.0089 (3)	1
O4	0.2602 (9)	0.9054 (7)	0.5995 (6)	0.0131 (3)	1
H(1a)	0.2200	0.0940	0.6140	0.050	0.5
H(1b)	0.2600	0.5260	0.8860	0.050	0.5
H2	0.0000	0.5000	0.5000	0.050	0.5

$U_{eq} = \frac{1}{3}\Sigma_i\Sigma_j U_{ij} a_i^* a_j^* a_i a_j$

Impedance measurements

The analysis of the frequency response of ac conductivity data was used to determine the superprotonic behavior of $Cs_2(HSO_4)(H_2AsO_4)$. Complex impedance measurements were performed using a compressed pellet of ~5 mm diameter and 2 mm thickness sintered at 293 K. Silver paint was evenly applied on both sides of the pellet for better electrical contact; the sample was then held between two spring-loaded electrodes. The electrical properties were collected under the stagnant air atmosphere and determined by impedance and modulus method using a frequency response analyzer (Hewlett-Packard 4192A LF). The impedance $|Z^*|$ and phase angle θ were measured with a computer interface. The frequency range was 100 Hz–13 MHz, and measurements were carried out at constant ranging from 373 to 473 K and maintained at ± 1 K accuracy by a Herrmann-Moritz 28480 controller for half an hour before collecting data.

Table 4 Anisotropic displacement parameters. The anisotropic displacement exponent takes the form exp.$[-2\pi^2\Sigma_i\Sigma_j U_{ij}h_ih_ja_ia_j*]$

Atoms	U_{11}	U_{22}	U_{33}	U_{12}	U_{13}	U_{23}
Cs	0.0261 (9)	0.0240 (8)	0.0287 (9)	−0.0003 (7)	0.0039 (5)	−0.0040 (7)
As	0.0170 (2)	0.0130 (19)	0.0151 (19)	−0.0017 (14)	0.0042 (13)	−0.0021 (14)
S	0.0170 (2)	0.0130 (19)	0.0151 (19)	−0.0017 (14)	0.0042 (13)	−0.0021 (14)
O1	0.0313 (5)	0.0316 (5)	0.0327 (15)	0.0076 (5)	0.0583 (4)	0.0011 (4)
O2	0.0491 (5)	0.0557 (6)	0.0364 (8)	−0.0082 (4)	0.0855 (4)	−0.0023 (4)
O3	0.0453 (7)	0.0461 (6)	0.0853 (6)	−0.0131 (5)	0.0783 (5)	−0.0031 (5)
O4	0.0246 (8)	0.0731 (6)	0.0365 (5)	0.0099 (5)	−0.0163 (5)	−0.0181 (5)

Results and discussion

Structural study

Description of the structure

At room temperature, the structure of $Cs_2(HSO_4)(H_2AsO_4)$ was found to be monoclinic with a unit cell very close to those in $Rb_2(HSO_4)(H_2PO_4)$ [10], $Cs_2(HSeO_4)(H_2AsO_4)$ [15], and $Rb_2(HSeO_4)(H_2PO_4)$ [20]. The crystal structure of $Cs_2(HSO_4)(H_2AsO_4)$ is built up from discrete $H_xS(As)O_4^-$ tetrahedra connected to zigzag chains via hydrogen bridges. Theses chains are linked by additional hydrogen bonds to a layer-like hydrogen bonding system.

Figure 1 shows a projection on the bc plane of $Cs_2(HSO_4)(H_2AsO_4)$. A projection on the ac plane is depicted in Fig. 2. This structure could be regarded as infinite (101) layers of hydrogen bonding joining the $H_xS(As)O_4^-$ groups into infinite chains along the [010] direction. From this description of the structure, we can notice that the atomic arrangement in $Cs_2(HSO_4)(H_2AsO_4)$ is similar to that in $Cs_2(HSeO_4)(H_2AsO_4)$, with a small decrease in the unit cell volume due to the small size of the S atom. The sulfate and arsenic atoms in CsHSAs are statistically disordered on one atomic position. The calculation in the non-centrosymmetric space group Pn also led to disordered atomic positions. In this monoclinic phase (room temperature), each S(As) atom is bonded to four oxygen neighbors that nearly form a slightly distorted tetrahedron. The S(As)O4 tetrahedra present three long distances (S/As–O2 = 1.578 (1) Å, S/As–O3 = 1.538 (3) Å, and S/As–O4 = 1.541 (2) Å) and one short bond (S/As–O1 = 1.485 Å). An important point in this

Fig. 1 Projection of $Cs_2(HSO_4)(H_2AsO_4)$ crystal structure along the a axis

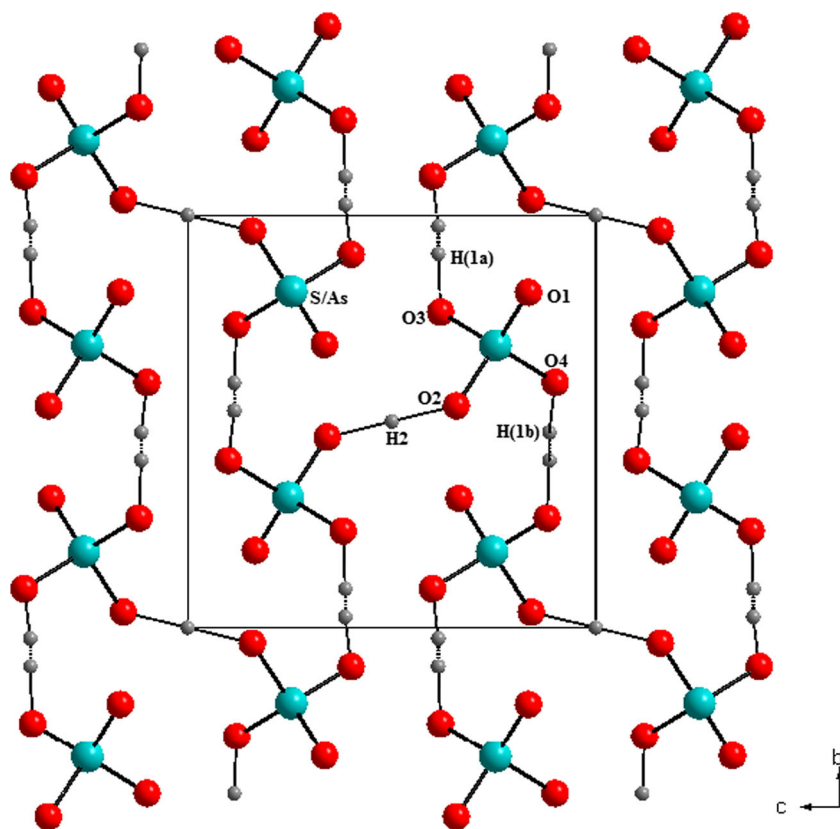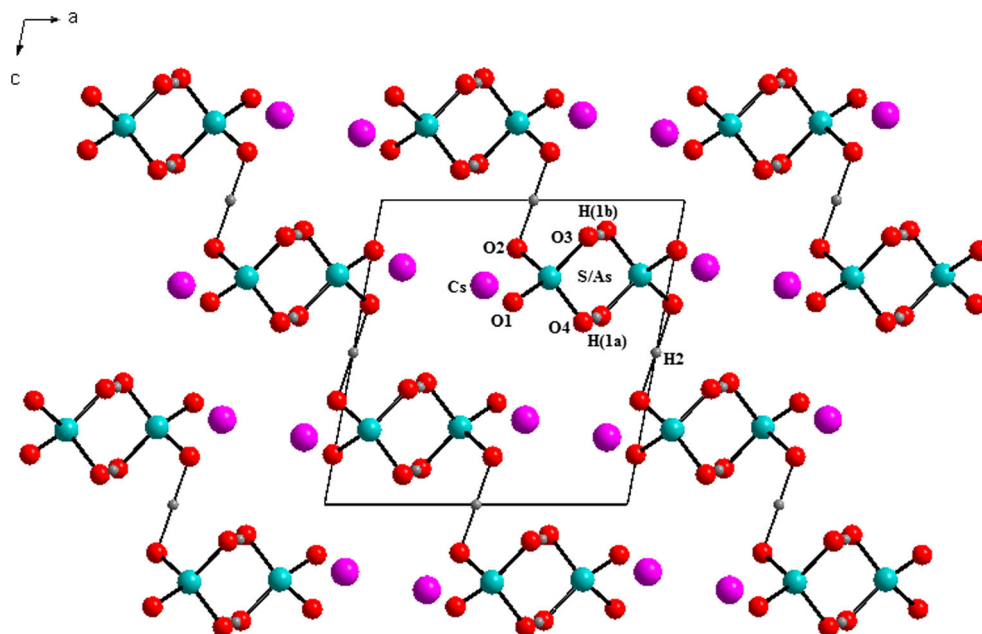**Fig. 2** Projection of Cs₂(HSO₄)(H₂AsO₄) crystal structure along the b axis

structure is that the mean value of S/As–O distances (1.552 Å) are intermediate between those of S–O distances (1.446 Å) in CsHSO₄ [21] and As–O distances (1.687 Å) in CsH₂AsO₄ [22]. The main interatomic distances and bond angles for the S(As)O₄ tetrahedron are given in Table 5.

In our investigation of this structure and previous works on this family of compounds [10, 15], it is possible to use differences in bond lengths to identify with which O in the O–O bond the proton is more highly associated. So, the localization of the hydrogen atoms based on the S/As–O bond distances and indications in the difference electron maps is in good agreement with the hydrogen bond net which can be deduced

from the short intermolecular O…O distances. The oxygen atoms O(2), O(3) and O(4) corresponding to the longest S/As–O bond distances can therefore be considered to belong to hydroxyl groups. In fact, the oxygen atom O(1) of the shortest S/As–O bond distances is not involved in any O–H bond. The O–S(As)–O angles range from 107.2 (7)° to 113.0 (7)°, indicating that the distortion of the S(As)O₄ tetrahedron is not so great (Table 5).

The cesium atom is coordinated by nine oxygen atoms. The Cs–O distances range from 2.976 (2) to 3.349 (6) Å. The next oxygen atom is 3.550 (2) Å further away from the cesium atom and cannot be considered as belonging to the coordination sphere of Cs. These nine coordinating oxygen atoms belong to six different S(As)O₄ tetrahedra. In comparison, the cesium atoms in CsHSO₄ and in CsH₂AsO₄ are coordinated by eight oxygen atoms, with Cs–O distances range from 3.105 to 3.503 Å [21] and from 3.056 to 3.259 Å [22], respectively.

The hydrogen bonding

Projection views of the title compound indicating the hydrogen bonding in Cs₂(HSO₄)(H₂AsO₄) are depicted in Figs. 1 and 2. Among the main geometrical feature of the hydrogen bond network reported in Table 5, it must be noted that all hydrogen atoms participate in the formation of hydrogen bonding. An examination of the intertetrahedral O–O bond lengths suggested the presence of two hydrogen bonds, the first one linking O(2) and O(2)^{IX}, and the second one linking O(3) and O(4). The proton coordinates were established from the location of peaks in Fourier difference maps in the vicinity of O(2)–O(2)^{IX} and O(3)–O(4). So, in the case of H(2), a peak was found at a distance of 1.280 (3) Å from O(2) and at the

Table 5 Bond distances (Å) and angles (°) in Cs₂(HSO₄)(H₂AsO₄) with standard deviations in parentheses

a. S/AsO₄ tetrahedron

S/As–O1	1.485 (2)	O1–O2	2.472 (2)	O1–S/As–O2	110.7 (7)
S/As–O2	1.578 (1)	O1–O3	2.491 (4)	O1–S/As–O3	113.0 (7)
S/As–O3	1.538 (3)	O1–O4	2.385 (5)	O1–S/As–O4	109.5 (7)
S/As–O4	1.541 (2)	O2–O3	2.555 (7)	O2–S/As–O3	107.9 (7)
		O2–O4	2.477 (6)	O2–S/As–O4	107.2 (7)
		O3–O4	2.490 (6)	O3–S/As–O4	108.3 (8)

b. Cesium coordination

Cs–O(1)^I	2.976 (2)	Cs–O(3)^V	3.010 (3)
Cs–O(1)^{II}	2.998 (1)	Cs–O(2)	3.043 (2)
Cs–O(2)^{III}	3.005 (2)	Cs–O(4)^{II}	3.265 (3)
Cs–O(1)	3.019 (1)	Cs–O(4)^{IV}	3.349 (6)
Cs–O(3)^{IV}	3.041 (3)	Cs–O(4)^{VI}	3.550 (2)

Symmetry codes: I: $-x + 3/2, y + 1/2, -z + 3/2$; II: $x + 1/2, -y + 3/2, z + 1/2$; III: $-x + 3/2, y - 1/2, -z + 3/2$; IV: $x + 1, y, z$; V: $x + 1/2, -y + 3/2, z - 1/2$; VI: $-x + 1, -y + 2, -z + 1$

inversion center (a special position) relating O(2) and O(2)[IX]. The angle formed between the S(As) atom, the O(2) atom, and this site, 115.20°, was close to the ideal tetrahedral value of 109.5°. The proton H(2) was thus taken to reside at this position and to have a fixed occupancy of 0.5. In the vicinity of O(3) and O(4), two Fourier difference peaks of comparable heights were found, one closer to O(3) and H(1a) atoms, and the other closer to O(4) and H(1b) atoms. The absence of a symmetry element relating the two O atoms indicated that H(1a) and H(1b) resides in two asymmetric potential minima between the oxygen atoms O(3) and O(4), and each of them has a fixed occupancy of 0.5. The distances $d_{O(3)-H(1a)}$ = 1.067 (3) Å and $d_{O(4)-H(1b)}$ = 0.932 (3) Å. The angles formed between the S(As) atom, the O atom, and potential sites [S(As)–O(3)–H(1a) = 114.24° and S(As)–O(4)–H(1b) = 116.62°] This results are in good agreement with the results obtained in the structure determination of $Rb_2(HSO_4)(H_2PO_4)$ by neutron powder diffraction [10] (Table 5) and with the chemical formula of the title compound that contains 1.5 protons per Cs atom, or three protons per formula unit.

The hydrogen bond O(3)–H(1a)…H(1b)–O(4) connects the $H_xS(As)O_4$ tetrahedra to zigzag chains parallel to the b direction (Fig. 1) with S(As)–S(As)–S(As) angles of 118.91°. Theses chains are linked by additional hydrogen bonds O(2)–H(2)–O(2)[IX] to a layer-like hydrogen bonding system (Fig. 2). The O–O bridges with distances between 2.525 (9) Å and 2.561 (3) Å belong to the strong hydrogen bonds [23] (Table 6).

Vibrational study

Although IR and Raman spectroscopy belong to the major physical methods of investigation of molecular structure, we have studied the IR and Raman spectra of the polycrystalline samples of CsHSAs, in order to confirm the presence of the two anions (SO_4^{2-} and AsO_4^{3-}) in the same crystal, and to elucidate the hydrogen bonds in their crystal lattice. The presence of two anions (S and As) at the same position as well as

the low symmetry of CsHSAs render a complete group factor analysis of this compound difficult. In this compound, the sulfate and arsenic tetrahedra deviate significantly from tetrahedral symmetry, which can be explained by the addition of protons to these tetrahedra. Consequently, the vibrational spectra are expected to differ in frequency values and intensities depending upon the symmetry. To make a qualitative assignment of the IR and Raman peaks to vibrational mode, we examine the modes and frequencies observed in similar hydrogen sulfate dihydrogen arsenate compounds [24, 25]. The infrared and Raman spectra of $Cs_2(HSO_4)(H_2AsO_4)$ at room temperature are shown in Fig. 3 and Fig. 4, respectively, and the observed IR and Raman bands are given in Table 7.

The IR and Raman spectra of CsHSAs that we obtained consist of a number of distinct and well-separated groups of bands, and can be divided into three frequency regions: 50–250 cm^{-1}, lattice mode; 250–1200 cm^{-1}, AsO_4^{-3} and SO_4^{-2} internal modes; and 1200–3700 cm^{-1}, high frequency hydrogen modes [26, 27]. The bands below 125 cm^{-1} in Raman spectra are due to external modes which contain the translations of Cs$^+$ [28] and lattice vibrations of AsO_4^{3-} and SO_4^{2-} anions [24]. The very weak lines between 125 and 200 cm^{-1} in Raman spectra probably correspond to the motion of O–H…O hydrogen stretching ($\nu_{o…o}$) and bending ($\delta_{o…o}$).

The low-frequency bonds are attributed to SO_4^{2-} and AsO_4^{3-} internal modes, in particular, the Raman bonds obtained at 278, 319 and 347 cm^{-1} are interpreted to $\nu_2(AsO_4)$ mode. We distinguish the $\nu_2(SO_4)$ by the medium broad and the strong Raman bands at about 446 and 479 cm^{-1}, respectively, and by the medium infrared bands near 478 cm^{-1}. The $\nu_4(AsO_4)$ mode is assigned to the medium broad and the two strong Raman bands observed in 389, 421, and 437 cm^{-1}.

The Raman bonds observed at 593 and 625 cm^{-1} are attributed to $\nu_4(SO_4)$ mode which is expected to be the strong peak in the IR spectrum at 598 cm^{-1}. The peaks observed in the region 804–864 cm^{-1} are associated to the $\nu_1(AsO_4)$ mode and those noted in the IR and Raman spectrum at 1043; 1094 cm^{-1} and 984; 1053 cm^{-1}, respectively, are presumed to result from $\nu_1(SO4)$. The $\nu_3(AsO_4)$ mode is observed in the

Table 6 Hydrogen bonding systems of $Cs_2(HSO_4)(H_2AsO_4)$, distances (Å), and angles (°)

O(d) –H–O(a)	O(d)…O(a) Å	O(d)–H Å	H…O(a) Å	O(d)–H…O(a) (°)
O(3)–H(1a) …O(4)[VII]	2.525(9)	1.067(3)	1.466(3)	171.9(8)
	2.533(7)	*1.070(2)*	*1.470(2)*	*171.0(2)*
O(4)–H(1b) …O(3)[VIII]	2.525(9)	0.952(3)	1.564(3)	168.7(8)
	2.533(7)	*0.960(2)*	*1.570(2)*	*167.0(2)*
O(2)–H(2) …O(2)[IX]	2.561(3)	1.280(3)	1.280(3)	180.0
	2.550(6)	*1.275(4)*	*1.275(4)*	

Entries given in italics refer to the results for the structure determination of $Rb_2(HSO_4)(H_2PO_4)$ [10] obtained by neutron powder diffraction

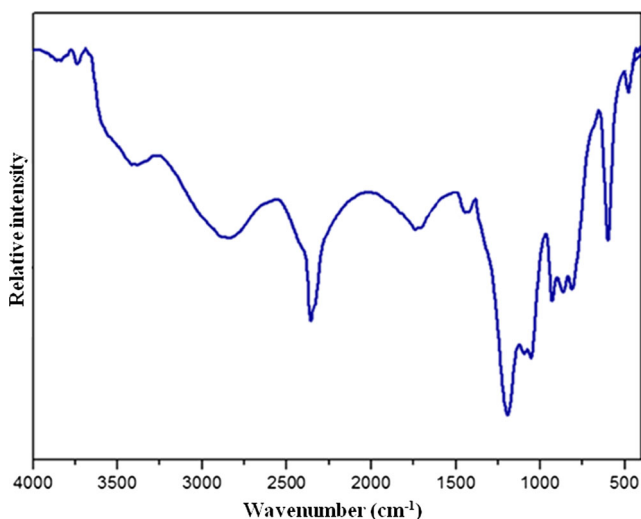Symmetry codes: VII: −x + 1/2, y − 1/2, −z + 3/2; VIII: −x + 1/2, y + 1/2, −z + 3/2; IX: −x + 1, −y + 2, −z + 2

Fig. 3 IR spectrum of $Cs_2(HSO_4)(H_2AsO_4)$ compound at room temperature

IR spectrum at about 931 cm^{-1} and at 923; 959 cm^{-1} in the Raman spectrum. The strong peak around 1180 cm^{-1} in IR spectra is tentatively attributed to the $\nu_3(SO4)$ mode and by the weak Raman bands near 1116 cm^{-1}.

The higher frequency IR peaks are attributed to reflect hydrogen modes [26, 27]. The corresponding OH stretching vibration give rise to characteristic broad trio bands of ABC type, associated to strongly hydrogen-bonded systems. These bands have been interpreted as OH stretching modes in Fermi resonance with combinations involving mainly OH bending vibrations or in terms of a strong coupling between fast OH and O…O stretching modes [29, 30]. The broad lines at 2843, 2358, and 1740 cm^{-1} in IR spectra can be assigned, respectively, to the ABC bands of OH stretching vibrations of both the short and the long hydrogen bonds in the
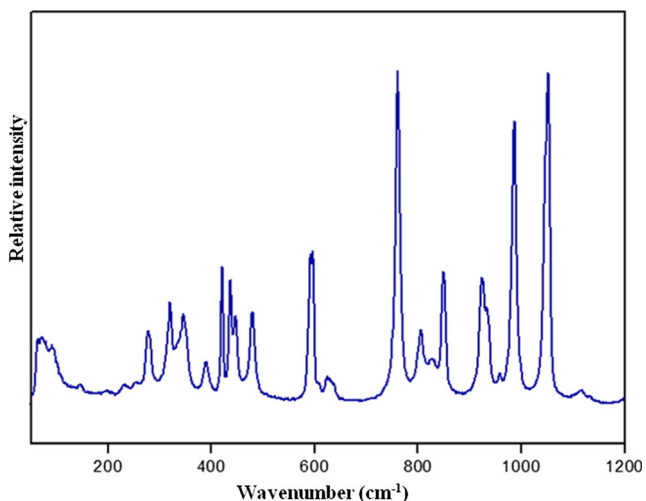
$Cs_2(HSO_4)(H_2AsO_4)$ compound. It is noted that the broadness of the ABC bands is due to a structural disorder [31].

Thermal behavior

The results of the high temperature behavior of (CsHSAs) are presented in Fig. 5. The differential scanning calorimetric (DSC) revealed that the title compound undergoes structural changes over the temperature 417 K with a calculated transition enthalpy $\Delta H_1 = 56.81$ J/g, which are unrelated to decomposition; its weight showed by the thermo-gravimetric curve (TGA) is stable to 480 K. This endothermic peak was also characterized by impedance and modulus measurements and was attributed to the superprotonic phase transition of (CsHSAs) materials. The high-temperature phase of $Cs_2(HSO_4)(H_2AsO_4)$ is thus "superprotonic" in nature.

The thermo-gravimetric (TG) curve shows that a first weight loss is followed by a plateau from 480 to 630 K accompanied with an important peak endothermic in the DSC curve at 534 K ($\Delta H_2 = 67.49$ J/g) correspond approximately to the departure of 1.5 molecules of water per chemical formula (calculated weight loss, 5.13 %). Taking account that the compound not containing water molecules in its structure, one can assume this weight loss is attributed to the decomposition of $Cs_2(HSO_4)(H_2AsO_4)$. The last weight loss is accompanied by endothermic peaks in the DSC curve at 841 K ($\Delta H_3 = 98.84$ J/g). At present, the nature of the volatile species that evolve at high temperature is unknown, but probably includes SO_x gases.

ac conductivity behavior

Four different formalisms are generally employed for analyzing the ac response of materials namely the complex dielectric constant ε^*, complex electric modulus M^*, complex impedance Z^*, and complex admittance G^*. We have used the Z^*, ε^*, and M^* representations to analyze the conductivity behavior. The following relations were used in evaluating the various quantities. The real part of impedance (Z') and the imaginary part (Z'') were directly measured in the frequency range 100 Hz–13 MHz.

The complex dielectric constant is:

$$\varepsilon^* = \frac{1}{j\omega C_0 Z^*} = \frac{1}{M^*} \tag{1}$$

with $\omega = 2\pi f$ and C_0 is the vacuum capacitance and where

$$\varepsilon^* = \varepsilon' + j\varepsilon'' \tag{2}$$

and

$$\tan\delta = \frac{\varepsilon''}{\varepsilon'} \tag{3}$$

Fig. 4 Raman spectrum of $Cs_2(HSO_4)(H_2AsO_4)$ compound at room temperature

Table 7 Observed Raman and IR frequencies (cm^{-1}) and band assignment at room temperature of $Cs_2(HSO_4)(H_2AsO_4)$

IR (cm^{-1})	I	Raman	I	Assignments
—		62	vw	
—		71	vw	Lattice vibrations of Cs^+, AsO_4^{3-}
—		91	vw	and SO_4^{2-}
—		145	sh	$\delta_{o\ldots o}$
—		230	sh	$\nu_{o\ldots o}$
—		278	w	
—		319	m	$\nu_2(AsO_4)$
—		347	m	
—		389	m	
—		421	s	$\nu_4(AsO_4)$
—		437	s	
—		446	mb	$\nu_2(SO_4)$
478	M	479	s	
598	S	593	vs	$\nu_4(SO_4)$
—		625	wb	
—		760	vs	
812	W	804	s	$\nu_1(AsO_4)$
—		826	sh	
864	W	849	s	
931	S	923	s	$\nu_3(AsO_4)$
—		959	vw	
—		984	vs	$\nu_1(SO_4)$
1043	Vw	1053	vs	
1094	Vw	—		
1180	S	1116	w	$\nu_3(SO_4)$
1428	B	—		$\delta(OH)$
1740 "C"	Vb	—		
2358 "B"	Wb	—		$\nu(OH)$
2843 "A"	Vb	—		
3404	Vb	—		
3736	B	—		$\nu(OH)$ of free H_2O of KBr
3854	Vb	—		

Relative intensities: *sh* shoulder, *w* weak, *vw* very weak, *wb* weak broad, *m* medium, *mb* medium broad, *b* broad, *vb* very broad, *s* strong, *vs* very strong, *sb* strong broad
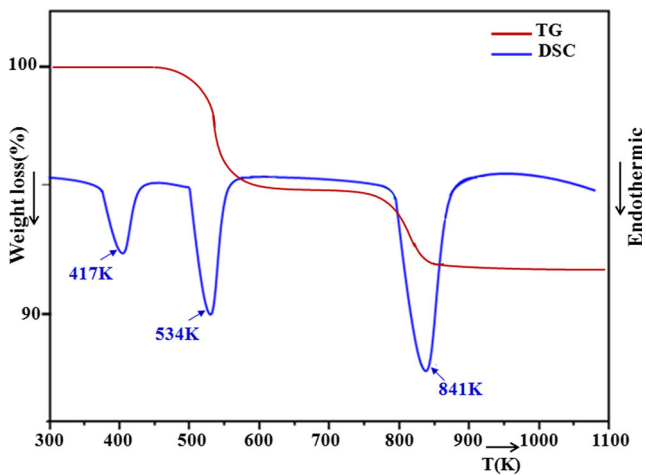
Fig. 5 The differential scanning calorimetry (*DSC*) and thermo-gravimetric analyses of Cs$_2$(HSO$_4$)(H$_2$AsO$_4$) compound

The real part of the electric modulus is

$$M' = \frac{\varepsilon'}{\left(\varepsilon'^2 + \varepsilon''^2\right)} \tag{4}$$

and the imaginary part of the electric modulus is

$$M'' = \frac{\varepsilon''}{\left(\varepsilon'^2 + \varepsilon''^2\right)}. \tag{5}$$

The ionic conductors (ICs) with point defects lead to a conductivity ranging up to 10^{-5} Ω^{-1} cm^{-1} whereas the superionic conductors (SICs) result in a conductivity of at least 10^{-4} Ω^{-1} cm^{-1}. The main difference between these two groups of materials concerns the activation energy (ΔE_σ): in the case of SICs, ΔE_σ is lower than 0.4 eV while in ICs, values varying between 0.6 and 1.2 eV are usually observed [32]. The superionic conductors have thus a high conductivity

Fig. 6 **a**, **b** Complex impedance diagrams –Z" versus Z' for Cs$_2$(HSO$_4$)(H$_2$AsO$_4$) at various temperatures
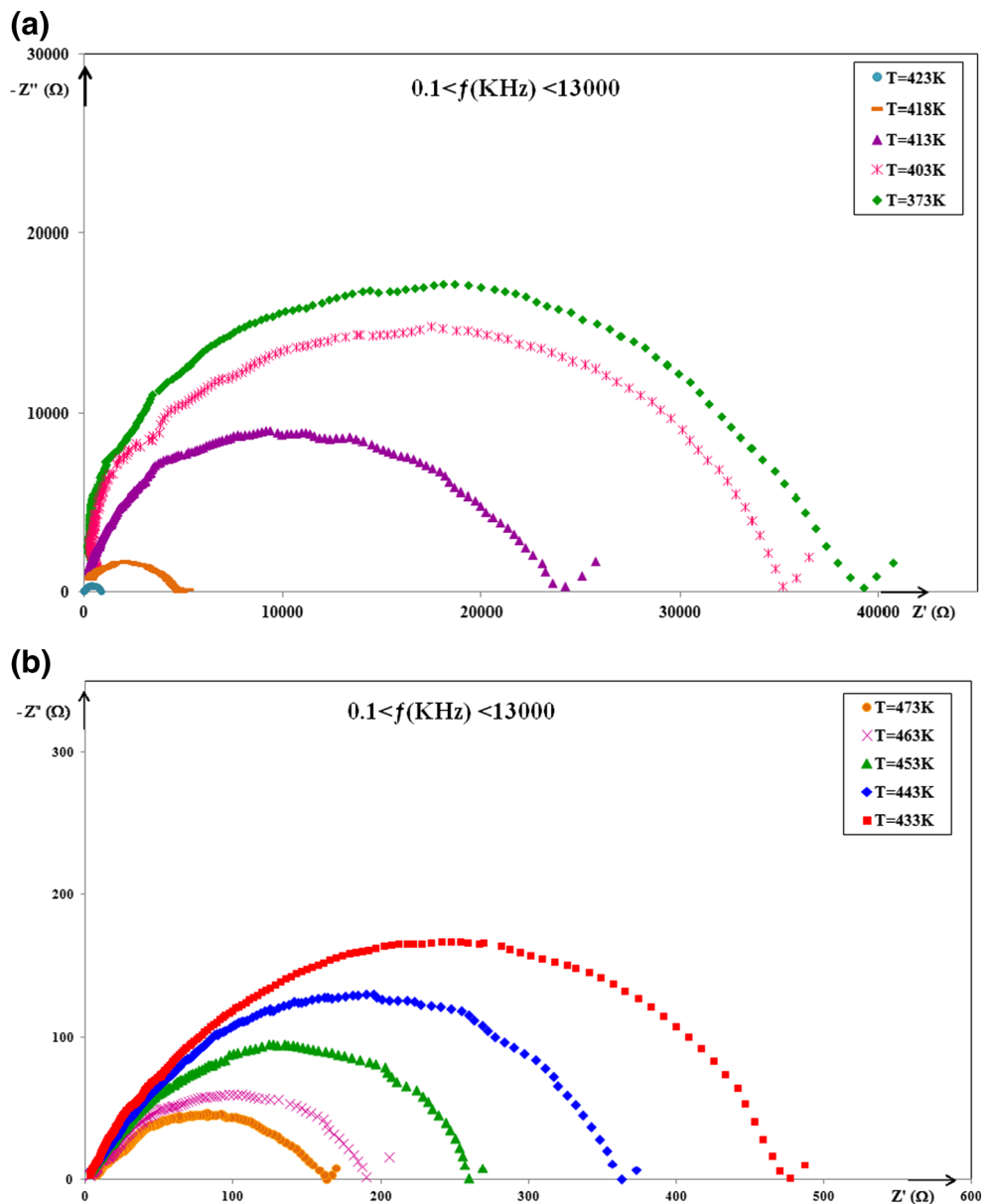
far below the melting point. This fundamental difference is due principally to the particular structures of SICs.

The temperature dependence of the protonic conductivity of $Cs_2(HSO_4)(H_2AsO_4)$ was determined from the analysis of the impedance spectroscopy at different temperatures. Complex plane plots of the complex impedance diagrams, $-Z''$ versus Z', at selected temperatures are shown in Figs. 6a, b in the low and high temperature phases, respectively. These impedance spectra show one non-ideal semicircle arc, which was attributed to the bulk properties and whose center is displaced below the real axis. This shows that (CsHSAs) follows the Cole-Cole law, and their extrapolation gives rise to an $[\alpha(\pi/2)]$ dispersion angle where $\alpha = 0.26$ is an empirical parameter ($0 \leq \alpha \leq 1$) proportional to the degree of deviation from the Debye model. The bulk ohmic resistance relative to each experimental temperature is the intercept on the real axis of the zero-phase angle extrapolation of the highest-frequency curve. The observed non-ideal semicircle was modeled using an equivalent circuit that contains one sub-circuit which consists of a resistance Rg, a capacitance Cg, and a constant phase element (CPE) connected in parallel which represents the grain response of the sample. These curves also show the temperature dependence of the resistance proving the superprotonic conduction properties of (CsHSAs).

The temperature dependence of the conductivity between 373 and 473 K is shown in Fig. 7, in a log(σT) vs 1000/T plot. Below 413 K, the protonic conductivity can be well described by the Arrhenius relation:

$$\sigma T = \sigma_0 \exp(-\Delta E_\sigma / kT) \tag{6}$$

With an activation energy equal to $\Delta E_\sigma = 0.47$ eV, where σ_0 is the pre-exponential factor, ΔE_σ is the activation energy for ion migration, and k is Boltzmann's constant. The conductivity jumped from 1.97×10^{-6} Ω^{-1} cm^{-1} at the temperature 373 K to 1.81×10^{-4} Ω^{-1} cm^{-1} at 433 K, characterizing the superprotonic conduction phase of the salt. The activation energy decreases from 0.47 eV ($T < 413$ K) at low temperature to 0.28 eV ($T > 423$ K) in the superionic phase, also such behavior shows the superprotonic conduction of (CsHSAs) [32]. The transition observed at 413 K corresponds to the structural transformation between the monoclinic phase and the superprotonic phase. Therefore, this transition which was revealed by thermo-differential measurement is well related to the hydrogen bonds in which the proton moves between the potential wells. Thus, the superionic phase transition corresponds to the melting of the proton sublattice reaching the "quasi-liquid" state where protons of the SO_4^{2-} and AsO_4^{3-} tetrahedral ions contribute to the unusually high conductivity as in the case of $CsHSO_4$ [1]. This behavior is characteristic of a plastic phase and implies a "free" rotation of HSO_4^- ions on given sites. In the superionic phase, a "quasi-liquid" state is manifested and both protons and cesium ions are disordered while in low temperature; the disorder is essentially confined to the protons. The drastic increase in conductivity by almost around twenty orders of magnitude on going from 413 K ($\sigma = 7.53 \times 10^{-6}$ Ω^{-1} cm^{-1}) to 423 K ($\sigma = 1.58 \times 10^{-4}$ Ω^{-1} cm^{-1}) is thus related to the high disorder of both sublattices.

Fig. 7 Temperature dependences of log (σT) and log fp = f (10^3/T), where fp is the M''max peak frequency, for $Cs_2(HSO_4)(H_2AsO_4)$
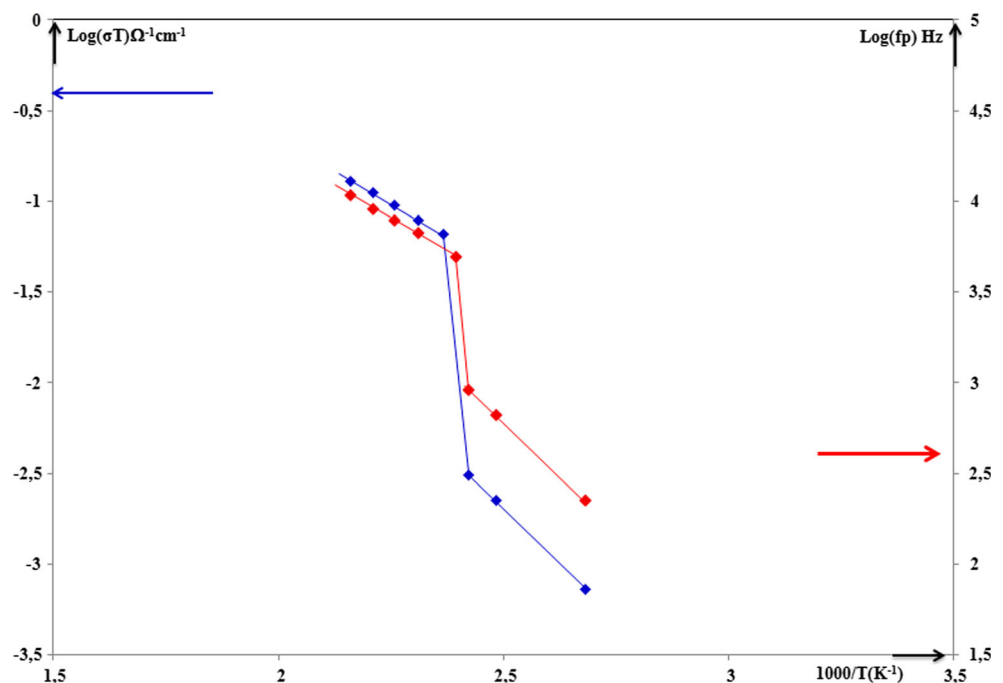
An analysis of the ion conductivity relaxation process in $Cs_2(HSO_4)(H_2AsO_4)$ has been undertaken in the complex electric modulus formalism:

$$M^* = M' + jM'' \tag{7}$$

This formalism is useful in determining the charge carrier parameters such as the conductivity relaxation time [23, 32]. For a temperature and a frequency given, the real part, M', and the imaginary part, M, of the M* complex modulus have been calculated from the complex impedance data

$$Z^* = Z' - jZ'' \tag{8}$$

by the following relations:

$$M' = \Omega C_0 Z'' \tag{9}$$

and

$$M'' = \Omega C_0 Z' \tag{10}$$

Isothermal frequency spectra, during heating process of the real, log M', and the normalized M''/M''_{max} imaginary part of the electric modulus for $Cs_2(HSO_4)(H_2AsO_4)$ versus log f are displayed in Figs. 8a, b, respectively. It is noticed that for all temperatures given, the real modulus M' tends to be a frequency-independent constant M'_∞ at high frequencies. At low frequencies, it decreases sharply (Fig. 8a), which indicates

Fig. 8 **a** Plots of log M' versus log f for $Cs_2(HSO_4)(H_2AsO_4)$ at various temperatures. **b** Plots of normalized modulus (M''/M''_{max}) versus log f for $Cs_2(HSO_4)(H_2AsO_4)$ compound at various temperatures
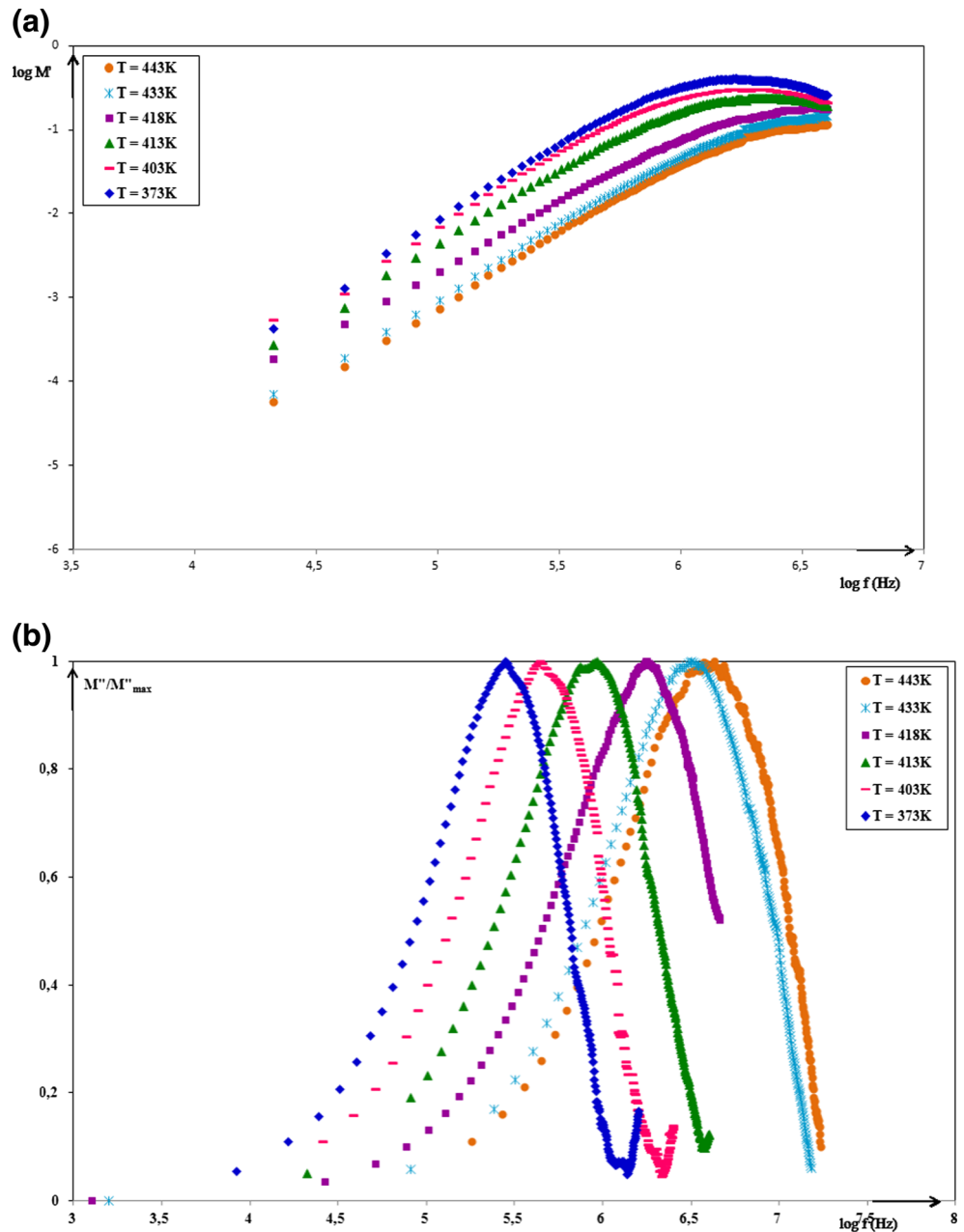
that the electrode polarization phenomena make a negligible contribution to M* and may be ignored when the electric data are analyzed in this form [33].

The M"/M"$_{max}$ spectrum relative to a given temperature shows an asymmetrical peak almost centered in the dispersion region of M' (Fig. 6b). The region to the left of the peak is where the H$^+$ protons are mobile over long distances whereas the region to the right is where the ions are spatially confined to their potential wells. It is clear from this figure that the maximum of the asymmetric peak shifts toward higher frequencies as the temperature is increased. The frequency range where the peak occurs is indicative of the transition from long-range to short-range mobility at increasing frequency and is defined by the condition $\Omega \tau_\sigma \approx 1$ where τ_σ is the most probable proton relaxation time. The M"/M"$_{max}$ curves are asymmetric, in agreement with the non-exponential behavior of the electrical function that is well described by the empirical stretched exponential Kohlrausch function

$$\varphi(t) = \exp.\left[-(t/\tau_\sigma)^\beta\right] \qquad (11)$$

[32], $0 < \beta < 1$ where β is the stretched exponential parameter. The smaller the value of β, the larger the deviation of the relaxation with respect to a Debye-type relaxation ($\beta = 1$). The full width at half maximum (FWHM) of the M"/M"$_{max}$ spectrum (1.3 decades) is greater than the breadth of a Debye–peak (1.14 decades) [34], and it results with an average value of $\beta = 0.87$ for the Kohlrausch parameter. This value of β clearly indicates that the relaxation is non-exponential.

In Fig. 7, we introduce the temperature dependence of log(fp), where

$$fp = 1/2\pi\tau_\sigma \qquad (12)$$

is the frequency relative to M"$_{max}$ peak corresponding to the bulk relaxation. An Arrhenius type law is shown with a noticeable jump at about 413 K and confirms the superprotonic transition already observed by measurements of conductivity and of thermo-differential analysis at the same temperature. At low and superprotonic phase temperature, both lines of the conductivity log (σT) and the modulus peak maxima log (fp) observed in the temperature studied are quasi-parallel, the activation energies deduced from the impedance (ΔE_σ) and modulus (ΔE_f) spectra are close ($\Delta E_{\sigma(L.T)} = 0.28$ eV; $\Delta E_{f(L.T)} = 0.27$ eV); $\Delta E_{\sigma(H.T)} = 0.47$ eV; $\Delta E_{f(H.T)} = 0.46$ eV in the temperature range 373–473 K), suggesting that the H$^+$ proton transport in (CsHSAs) is probably due to a hopping mechanism [35].

On the other hand, the value of the FWHM of peaks (Fig. 6b) corresponding to various temperatures is approximatively close to an average value of 1.3 decades. Consequently, β may be considered as an independent of temperature in the temperature studied range. The value of the β parameter, smaller than 1, can be attributed to the existence of a distribution of relaxation times in the compound. Such an interpretation has been adopted for many solid electrolytes [1–3]. On the contrary, recent studies based on the overlapping of the log M' vs. log f and log M" vs. log f plots obtained for various temperatures have shown that this interpretation was questionable [32].

Conclusion

Chemical preparation and crystal structure are described for a new mixed dicesium hydrogen sulfate dihydrogen arsenate salt $Cs_2(HSO_4)(H_2AsO_4)$. The structure is determined by a single-crystal X-ray analysis, and shows that this compound crystallizes in a monoclinic system P2$_1$/n. This structure is characterized by disordered H_xS/AsO_4^- tetrahedra connected to zigzag chains via hydrogen bridges along the [010] direction. These chains are linked by additional hydrogen bonds to a layer-like hydrogen bonding system parallel (10$\bar{1}$). The O…O bridges with distances between 2.525 and 2.561 Å belong to the strong hydrogen bonds. Cesium atoms have nine oxygen atom neighbors. The main feature of this structure is the coexistence of two different anions (H_2AsO_4 and HSO_4) in the same crystal structure, and the ratio of sulfate-arsenate is 1:1. The infrared and Raman spectrum of the title compound was acquired at room temperature and is characterized by the apparition of a few bonds which confirm the presence of these two different anions. The thermo-differential analysis shows three anomalies at 417, 534, and 841 K. The first one corresponds to a superprotonic phase transition. The dehydration steps are revealed by the thermo-gravimetric analysis which indicates that the weight of (CsHSAs) is stable to ~480 K; this shows that the transition at 417 K is unrelated to decomposition. From ac impedance measurements, both conductivity and modulus spectra of this compound were analyzed at low and high frequency in the 373–473 K temperature range. The relaxation conductivity is well described by the empirical, stretched exponential Kohlrausch function $\varphi(t) = \exp.[-(t/\tau_\sigma)^\beta]$. Information about charge carrier transport mechanism is obtained by comparison of ΔE_f with ΔE_σ.

The activation energies for the $Cs_2(HSO_4)(H_2AsO_4)$ compound calculated respectively from the modulus and impedance spectra are approximately close, suggesting that the protonic transport above and below the superprotonic phase transition (417 K) is probably due to a hopping mechanism.

References

1. Baranov AI, Merinov BV, Tregubchenko AB, Shuvalov LA, Shchagina NM (1988) Phase Transitions, structure, protonic conductivity and dielectric properties of $Cs_3H(SeO_4)_2$ and $Cs_3(H, D)(SeO_4)_2$. Ferroelectrics 81:187–191

2. Baranov AI, Tregubchenko AV, Shuvalov LA, Shchagina NM (1987) Structural phase transitions and proton conductivity of $Cs_3H(SeO_4)_2$ and $(NH_4)_3H(SeO_4)_2$ crystals. Sov Phys, Solid State 29:1448–1449

3. Belushkim AV, Adams MA (1997) Lattice dynamics of KH_2PO_4 at high pressure. Physica B 234-236:37–39

4. Kreuer KD (1996) Proton conductivity: materials and applications. Chem Matter 8:610–641

5. Zhu B, Albirsson I, Mellander BE, Meng G (1999) Intermediate-temperature proton-conducting fuel cells—present experience and future opportunities. Solid State Ionics 125:439–446

6. Guin M, Tietz F (2015) Survey of the transport properties of sodium superionic conductor materials for use in sodium batteries. Power Sources 273:1056–1064

7. Bouchet R, Miller S, Duclot M (2001) A thermodynamic approach to proton conductivity in acid-doped polybenzimidazole. Solid State Ionics 145:69–78

8. Chisholm CRI, Haile SM (1999) Structure and thermal behavior of the new superprotonic conductor $Cs_2(HSO_4)(H_2PO_4)$. Acta Crystallogr B55:937–946

9. Averbuch-Pouchot MT, Durif A (1980) Crystal structure of $KHSO_4 \cdot KH_2PO_4$. Res Bull 15:427–430

10. Stiewe A, Sonntag R, Troyanov SI, Hansen T, Kemnitz E (2000) Synthesis and structure determination of $Rb_2(HSO_4)(H_2PO_4)$ and $Rb_4(HSO_4)_3(H_2PO_4)$ by x-ray single crystal and neutron powder diffraction. Sol State Chem 149:9–15

11. Averbuch-Pouchot MT (1981) Hydrogen bonding in $NH_4HSO_4 \cdot NH_4H_2PO_4$. Mater Res Bull 16:407–411

12. Boubia M, Averbuch-Pouchot MT, Durif A (1985) Ordered AsO_4 and SO_4 tetrahedra in diammonium trihydrogenarsenate sulfate. Acta Crystallogr C41:1562–1564

13. Matsuo Y, Hatori J, Nakashima Y, Ikehata S (2004) Superprotonic and ferroelastic phase transition in $K_3H(SO_4)_2$. Solid State Commun 130:269–274

14. Noda Y, Uchiyama S, Kafuku K (1990) Structure analysis and hydrogen bond character of $K_3H(SO_4)_2$. Phys Soc Jpn 59:2804–2810

15. Jaouadi K, Zouari N, Mhiri T, Giorgi M (2009) Synthesis, structural study and thermal behaviour of a new superprotonic compound: $Cs_2(HSeO_4)(H_2AsO_4)$. Phys Procedia 2:1185–1194

16. Sheldrick GM (1995) SORTAV user guide. University of Göttingen, Göttingen

17. International Tables for X-ray Crystallography Vol. C (1992). Kluwer Academic Publishers, Dordrecht

18. Sheldrick GM (1990) SHELXS-97, program for the solution of crystal structures. University of Göttingen, Göttingen

19. Sheldrick GM (1997) SHELXL-97, program for crystal structure determination. University of Göttingen, Göttingen

20. Zouari N, Jaouadi K, Mhiri T, Giorgi M (2005) X-ray single crystal, vibrational and phase transitions in the mixed $Rb_2(HSeO_4)(H_2PO_4)$. Phase Transit 78:627–638

21. Itoh K, Ukeda T, Ozaki T, Nakamura E (1990) Redetermination of the structure of caesium hydrogensulfate. Acta Crystallogr C46:358–361

22. Pakhomov VI, Sil'nitskaya GB, Semin GK, Gerken VA, Kalashnikova II (1985) Structural perfection of CsH_2AsO_4 crystals. Inorg Mater 21:142–143

23. Novak A (1974) Hydrogen bonding in solids correlation of spectroscopic and crystallographic data. Struct Bond 18:177–216

24. Amri M, Zouari N, Mhiri T, Pechev S, Gravereau P, Von Der Muhll R (2007) Structural, vibrational and dielectric properties of new potassium hydrogen sulfate arsenate: $K_4(SO_4)(HSO_4)_2(H_3AsO_4)$. Phys Chem Solids 68:1281–1292

25. Naili H, Mhiri T, Jaud J (2001) Crystal structure and characterization of $CsH_5(AsO_4)_2$: a new cesium pentahydrogen arsenate, and comparison with $CsH_5(PO_4)_2$ and $RbH_5(AsO_4)_2$. Sol State Chem 161:9–16

26. Le Calve N, Romain F, Limage MH, Novak A (1989) Etude par spectroscopic Raman et infrarouge des verres de pseudo-spin $Rb_{0,65}(NH_4)_{0,35}H_2PO_4$. Mol Struct (Theochem) 200:131–147

27. Romain F, Novak A (1991) Raman study of the high-temperature phase transition in CsH_2PO_4.Molecular. Structure 263:69–74

28. Naili H, Mhiri T, Daoud A (1999) Crystal structure, characterisation and vibrational study of a mixed compound $Cs_{0.4}Rb_{0.6}H_2PO_4$. Phase Transit 71:271–286

29. Marchon B, Novak A (1983) Vibrational study of CsH_2PO_4 and CsD_2PO_4 single crystals. Chem Phys 78:2105–2120

30. Hubert Joe I, Jayakumar VS, Aruldhas G (1995) FT-IR and polarized Raman spectra of $N(CH_3)_4H_2PO_4 \cdot H_2O$. Sol State Chem 120:343–352

31. Fillaux F, Marchon B, Novak A (1984) Raman OH stretching band shape of and proton dynamics in CsH_2PO_4. Chem Phys 86:127–136

32. Colomban P (1992) Proton conductors: solids, membranes, and gels materials and devices. Cambridge University Press, Chemistry of Solid State Materials

33. Howell FS, Bose RA, Macedo PB, Moynihan CT (1974) Electrical relaxation in a glass-forming molten salt. Phys Chem 78:639–648

34. Martin SW, Angell CA (1986) Dc and ac conductivity in wide composition range $Li_2O-P_2O_5$ glasses. Non-Cryst Solids 83:185–207

35. Chowdari BVR, Gopalakrishnan R (1987) ac conductivity analysis of glassy silver iodomolybdate system. Solid State Ionics 23:225–233